Available online at www.sciencedirect.com
ScienceDirect
International Journal of Heat and Mass Transfer 50 (2007) 405–411
International Journal of HEAT and MASS TRANSFER
www.elsevier.com/locate/ijhmt

Thermal conductivity of a metal-organic framework (MOF-5): Part II. Measurement

B.L. Huang [a], Z. Ni [b], A. Millward [b], A.J.H. McGaughey [a], C. Uher [c], M. Kaviany [a,*], O. Yaghi [b]

[a] Department of Mechanical Engineering, University of Michigan, Ann Arbor, MI 48109-2125, USA
[b] Department of Chemistry, University of Michigan, Ann Arbor, MI 48109-1055, USA
[c] Department of Physics, University of Michigan, Ann Arbor, MI 48109-1040, USA

Received 2 March 2006; received in revised form 29 September 2006
Available online 7 November 2006

Abstract

The thermal conductivity of MOF-5 single crystals is measured over a wide temperature range between 6 K and 300 K, using the longitudinal, steady-state heat flow method. Between 6 K and 20 K, the thermal conductivity increases with the increase in temperature and exhibits a peak near 20 K. This peak results from the crossover between the decreasing mean free path and the increasing phonon specific heat with the increasing temperature. From 20 K to 100 K, the thermal conductivity decreases rapidly with increasing temperature. Above 100 K, the thermal conductivity is nearly temperature independent, and its value at 300 K is 0.32 W/m K, a rather low value for crystals. The mean free path analysis shows that at high temperature, the phonon mean free path is minimized to the cage size due to the porous, flexible structure of MOF-5.

Keywords: Metal-organic framework; Measurement; Thermal conductivity; Nanoporous crystals

1. Introduction

The crystalline metal-organic frameworks (MOFs) are a new sub-family of the nanoporous crystals. They are currently receiving attentions because of their high adsorption surface area and large free cage volume [1,2]. MOFs are most attractive for their high capacity for hydrogen absorption and storage [3]. Many members of the MOF family are synthesized in recent years. Unlike other nanoporous crystals with inorganic host frameworks, MOFs have three-dimensional hybrid frameworks, which are comprised of metal-oxygen cages connected by a variety of organic bridges and lead to designable pore size, shape and functionality [3]. MOF-5, is the first stable cube-like structure in the family. MOF-5 has a regular, three-dimensional cubic lattice with 1,4-benzenedicarboxylate (BDC) as edges and Zn_4O cluster as vertexes (see Fig. 1). The thermal properties of MOF-5 are important for gas storage and other potential applications.

Microporous crystals, such as zeolites, characterized by large unit cells and angstrom sized pores and linkers, normally have very low thermal conductivities [4–6]. Generally these crystals cannot be grown to a big-size single crystal and their thermal conductivities are often extracted indirectly from the measurement of loose or compacted powder [4]. Since there are many factors affecting the effective thermal conductivity and currently no model can account for all of them, the uncertainty in the effective crystal thermal conductivity is large [4]. MOF-5, however, has been grown up to a linear dimension of 1–2 mm, making the direct measurement possible. MOF-5 has a longer linker and a larger pore size, compared to most nanoporous crystals (including zeolites). For example, the number density of MOF-5 is 2.46×10^{28} atoms/m^3, much less than those

* Corresponding author. Tel.: +1 734 936 0402; fax: +1 734 647 3170.
E-mail address: kaivany@umich.edu (M. Kaviany).

0017-9310/$ - see front matter © 2006 Elsevier Ltd. All rights reserved.
doi:10.1016/j.ijheatmasstransfer.2006.10.001

Nomenclature

d	distance
k	thermal conductivity
l	distance, length
u	sound speed
A	cross area
D	diameter
H	height
J	current
Q	heat flow
T	temperature

Greek symbols

ϵ	emissivity
λ	mean free path
σ	Stefan–Boltzmann constant
φ	voltage

Subscripts

ch	chromel
con	constantan
cu	copper
g	group
h	heater
loss	loss
p	phonon
D	Debye

of zeolites [sodalite (5.13×10^{28} atoms/m^3) and zeolite-A (4.10×10^{28} atoms/m^3)] [7]. Therefore, MOF-5 is expected to have a even lower thermal conductivity than most nanoporous crystals. Also, the special cage–bridge structure of MOF-5 makes it an ideal object to study the effects of the cage and bridge structure on the microscale energy transport. Considering the freedom in the construction of MOFs [3], such a study may lead to the first step in the systematic design of structures with the desired thermal properties.

Here we report the measurement of the thermal conductivity of MOF-5 over a wide temperature range, from 6 K to 300 K, using the longitudinal, steady-state heat flow method. Then the low thermal conductivity of MOF-5, and its weak temperature dependence at high temperature, are discussed, which are shown to be due to the minimization of the phonon mean free path.

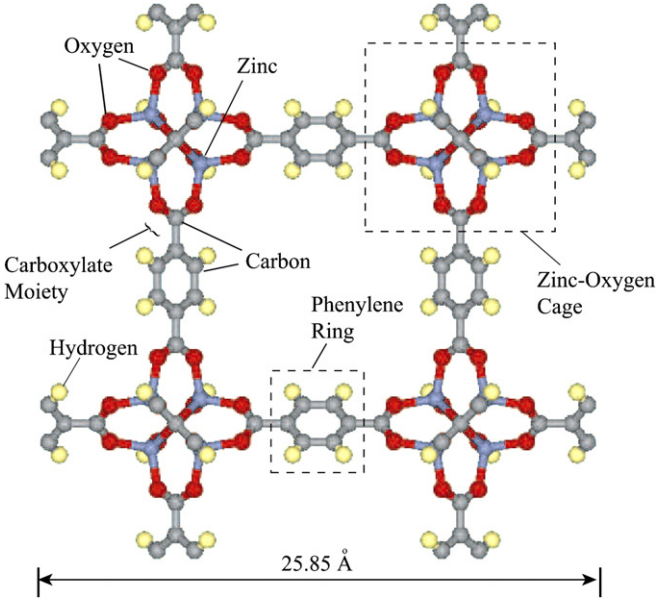

Fig. 1. The cubic structure of MOF-5. The lattice constant at 300 K is 25.85 Å. The diameter of the cage is 7.16 Å.

2. Experiment

2.1. Crystal preparation

We synthesized large single cubic crystals by mixing 8.38 g $Zn(NO_3)2 \cdot 4H_2O$ (32.0 mmol) and 1.77 g terephthalic acid (10.7 mmol) dissolved in 100 mL DEF in a glass beaker and sonicating the mixture for 15 min. The solution was dispensed evenly into 20 scintillation vials (20-mL size) by using a plastic syringe equipped with a PTFE filter (Whatman, 0.45 μm pore size). The vials were then tightly capped and placed in an isothermal oven. The reactions were stopped after being heated at 368 K for 72 h. The mother liquor in each vial was decanted while warm and the product was washed with fresh DEF (3×5 mL for each vial). In a typical batch as described above, 5–6 large single cubic crystals (size 1–2 mm) were obtained. The cubic crystals were confirmed to be MOF-5 by the coincidence of experimental PXRD pattern with the simulated one and by examination of these crystals under an optical microscope [8,2,3].

After obtaining the large single cubic crystals, solvent-exchange was carried out to remove the high-boiling-point DEF in the crystals. The suitable crystals were collected in a 20-mL scintillation vial. After the DEF solvent was removed as clean as possible by using a pipette, this open vial was placed in a desiccator saturated with chloroform vapor, which slowly condensed into the vial and accumulated to 5 mm tall in 3 days. After the removal of the accumulated chloroform, two different methods were adopted for further solvent-exchange. One was to fill the vial with chloroform liquid and then cap it (direct addition of chloroform liquid). The solvent volume was replaced twice after a 1-day and a 2-day immersion respectively, and was kept at rest for another 2 days. The total time of

Table 1
Characteristics of the samples used

Sample	Size (mm^3)	Chemical preparation
◇	$0.94 \times 1.13 \times 1.32$	Old solvent, solvent-exchange: direct addition of chloroform liquid
□	$1.71 \times 1.17 \times 1.79$	Fresh solvent, solvent-exchange: slow condensation of chloroform vapor
○	$1.33 \times 0.83 \times 1.50$	Fresh solvent, solvent-exchange: slow condensation of chloroform vapor
△	$0.75 \times 1.13 \times 1.20$	Fresh solvent, solvent-exchange: slow condensation of chloroform vapor

chloroform-exchange of large MOF-5 single crystals was 3 days in desiccator and 5 days on bench. The other method was to repeat the vapor diffusion exchange (slow condensation of chloroform vapor) 3 times in 7 days. The latter method is easier for obtaining clear crystals. The effectiveness of exchanging DEF solvent was confirmed by the disappearance of characteristic amide carbonyl peaks in FT-IR spectra. Table 1 shows the characteristics of the crystal samples used in the conductivity measurement. Both the stored (old) solvent and the fresh solvent were purified and both solvent-exchange methods were used.

2.2. Thermal conductivity measurement

The thermal conductivity of the MOF-5 samples was measured on the basis of the Fourier law [9], using the longitudinal, steady-state heat flow method [10,11]. Since MOF-5 has a cubic structure, its thermal conductivity is isotropic and can be obtained by the measurement in only one direction. Fig. 2(a) shows the apparatus used for the measurement and Fig. 2(b) shows the thermal circuit diagram for the heat flow paths.

To avoid the formation of small cracks resulting from the adsorption of water vapor, the MOF-5 sample was prepared in a sealed airbag with filling prepurified nitrogen atmosphere. The dimensions of the sample were measured using a microscope. Two fine copper-constantan thermocouples (the diameters of the copper and constantan wires are 30 μm and 10 μm, respectively) were attached to the surface of the sample, using SE4422, a fast-drying thermally conductive adhesive produced by Dow Corning. The distance d between the two thermocouple centers was also measured using the microscope. Then the sample was mounted between a small heater and the copper heat sink of a cryostat, as shown in Fig. 2(a). Two copper wires with diameters of 30 μm were used for current input to the heater, and two chromel wires with diameters of 10 μm were used to measure the heater voltage. The lengths of the copper and chromel wires are all 25 cm (long enough to minimize the conduction loss). The cryostat was then evacuated until the pressure was reduced to 10^{-7} torr. Liquid nitrogen was used to cool the sample from 300 K to about 100 K. Then liquid helium was used to cool the sample to 6 K. Thereafter, the temperature of the sample was raised incrementally back to 300 K. The thermal conductivity was measured during the procedure. The cooling rate using liquid helium is fast and the resulting thermal

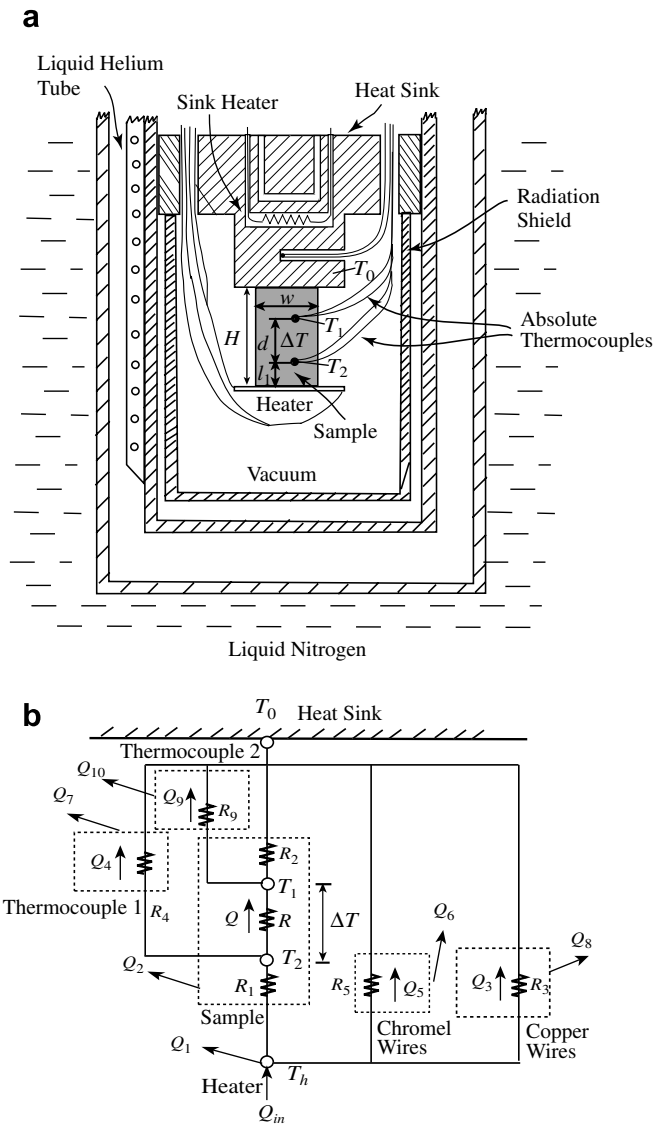

Fig. 2. (a) The apparatus for the measurement of thermal conductivity. (b) The thermal circuit diagram [9] for the heat flow path through the sample and various other paths.

stress may lead to the formation of defects within the sample, which may affect the low temperature results.

The specification of the thermal conductivity involved two steps. First, at each predetermined temperature point, a 1 mA DC current was input into the heater. After 5–10 min (to allow for steady, stable readings), when the outputs of the thermocouples became stable, the input current J_h, the voltage $\Delta\varphi_h$ and the temperature difference ΔT were recorded. After finishing the first step, the sample was

detached from the heat sink, and left suspended by thermocouple wires, while keeping the heater attached to its bottom surface. The sample was then placed back into the cryostat and the cryostat was evacuated and cooled again. At the same temperature points as in the first step, the input current of the heater was adjusted by trial and error to raise the temperature of the sample to the same average temperature measured in the first step. The corresponding current $J_{e,2}$ and voltage $\Delta\varphi_{h,2}$ of the heater were recorded and the heat loss Q_{loss} was calculated by $Q_{loss} = J_{e,2}\Delta\varphi_{h,2}$.

Then the thermal conductivity k was calculated by

$$k = \frac{(J_h\Delta\varphi_h - Q_{loss})d}{A\Delta T}, \tag{1}$$

where A is the cross-section area perpendicular to the heat flow.

2.3. Heat loss model

We used the measured heat loss in Eq. (1) at high temperatures (above 100 K). However, at low temperatures (below 100 K), the liquid helium ran out before the time-consuming heat loss measurement was completed. This measurement is also rather challenging due to the potentially unstable outputs of thermocouples at low temperatures. So for low temperatures (below 100 K), we used a model to calculate the heat loss. This model can also guide minimizing the error due to the heat loss.

From Fig. 2(b), Q_{loss} is defined as the part of input heat flow that cannot reach the cold cross-section (with temperature T_1) and it is the summation of Q_1 to Q_8, i.e.,

$$Q_{loss} = \sum_{i=1}^{8} Q_i, \tag{2}$$

where Q_1 is the radiation heat loss from the heater surface, Q_2 is the radiation heat loss from the sample surface, Q_3, Q_4, and Q_5 represent the conduction through the copper wires (heater), thermocouple wires, and chromel wires, and Q_6, Q_7 and Q_8 are the radiation from the chromel wires, thermocouple wires and the copper wires (heater) surface.

We assumed the temperature varied linearly along the sample surface and the wires. Then each Q_i ($i = 1, 2, \ldots, 8$) can be calculated from

$$Q_1 = \sigma\varepsilon_h A_h (T_h^4 - T_0^4), T_h = \frac{l_1(T_2 - T_1)}{d} + T_2$$

$$Q_2 = \sigma\varepsilon_s \int_0^{l_1+d} 2(w+l)\left(\left(T_1 + \frac{(T_2 - T_1)x}{d}\right)^4 - T_0^4\right)dx$$

$$Q_3 = 2k_{cu}\frac{\pi D_{cu}^2}{4}\frac{(T_h - T_0)}{l_{cu,h}}$$

$$Q_4 = k_{cu}\frac{\pi D_{cu}^2}{4}\frac{(T_2 - T_0)}{l_{cu,s}} + k_{con}\frac{\pi D_{con}^2}{4}\frac{(T_2 - T_0)}{l_{con,s}}$$

$$Q_5 = 2k_{ch}\frac{\pi D_{ch}^2}{4}\frac{(T_h - T_0)}{l_{ch,h}}$$

$$Q_6 = 2\sigma\varepsilon_{ch}\int_0^{l_{ch,h}} \pi D_{ch}\left\{\left[T_0 + \frac{(T_h - T_0)x}{d}\right]^4 - T_0^4\right\}dx$$

$$Q_7 = \sigma\varepsilon_{cu}\int_0^{l_{cu,s}} \pi D_{cu}\left\{\left[T_0 + \frac{(T_2 - T_0)x}{d}\right]^4 - T_0^4\right\}dx + \sigma\varepsilon_{con}\int_0^{l_{con,s}} \pi D_{con}\left\{\left[T_0 + \frac{(T_2 - T_0)x}{d}\right]^4 - T_0^4\right\}dx$$

$$Q_8 = 2\sigma\varepsilon_{cu}\int_0^{l_{cu,h}} \pi D_{cu}\left\{\left[T_0 + \frac{(T_h - T_0)x}{d}\right]^4 - T_0^4\right\}dx, \tag{3}$$

where σ is the Stefan–Boltzmann constant, A_h is the area of the heater, ε_h, ε_s, ε_{cu}, ε_{con}, and ε_{ch}, are the emissivities of the heater, sample, copper, constantan and chromel, respectively (all assumed constant). Also, k_{cu}, k_{con} and k_{ch} are the thermal conductivities of copper, constantan and chromel, respectively (all are temperature dependent). Here l_1 is the distance from the hot cross-section to the heater, w and l are the width and length (not shown) of the sample, $l_{cu,h}$ and $l_{ch,h}$ are the lengths of the copper and the chromel wires connected to the heater, respectively, and $l_{con,s}$ and $l_{cu,s}$ are the lengths of the constantan and the copper wires of the thermocouples. Also, D_{cu}, D_{ch} and D_{con} are the diameters of the copper, the chromel and the constantan wires, respectively. The outputs of the thermocouples give the temperature of cold cross-section T_1 and that of hot cross-section T_2, T_0 is the temperature of the heat sink and the surroundings, and T_h is the temperature of the heater as obtained by extrapolation from the linear temperature distribution between the hot and cold cross-sections.

It is assumed that the effect of thermal expansion and the contact resistance are negligible, and that temperature varies linearly along the longitudinal direction. Based on the temperatures of the heater and sink and the dimensions of the heater and sample, the radiation through the sample is negligible (less than 1% of the total heat flow at 300 K) due to the low temperatures and the small view factor (less than 0.1).

Fig. 3 shows the ratio $Q_i/J_h\Delta\varphi_h$, as a function of ambient temperature T_0. The emissivity of the wires was estimated by comparing the model prediction with the measured heat loss, using a sample (e.g., glass) with similar dimensions and a known thermal conductivity. We found the best fit using 0.6 for the copper wires, 0.6 for the constantan wires, 0.6 for the chromel wires, and 1.0 for the heater (note these data for wires depend on the dielectric coating on the wires). The emissivity of the sample is assumed to be 1.0, giving the best fit with the measured heat loss at 300 K (actually, the choice of the emissivity of the sample is not critical because the radiation heat transfer from the sample is small, as shown below). The temperature-dependent thermal conductivities of constantan, chromel, and copper were from [12]. As shown in Fig. 3, above 100 K, the total heat loss is dominated by

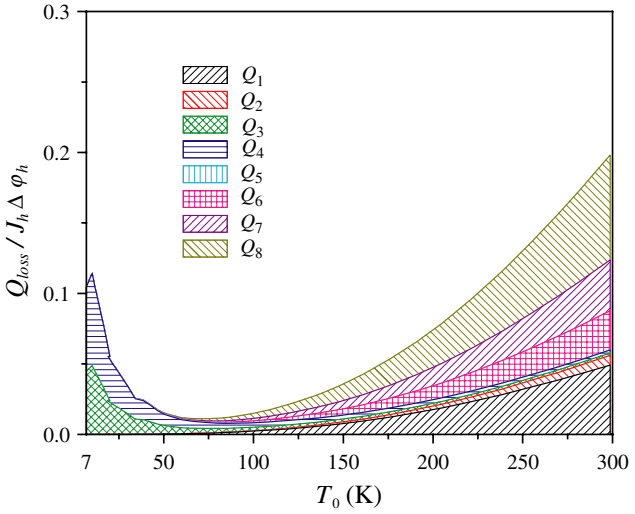

Fig. 3. The predicted contribution of the different heat losses as a function of ambient temperature, for a typical experiment. The geometric parameters in this heat loss model, are set as those for a typical sample at room temperature. The temperatures, T_1 and T_2, are set as the measured values at the ambient temperature T_0.

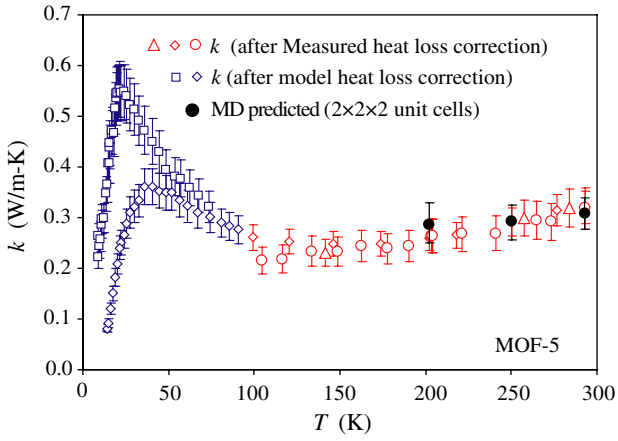

Fig. 4. Variation of the MOF-5 thermal conductivity with respect to the temperature. Below 100 K, the heat loss correction is made by the heat loss model. The MD predicted result of $2 \times 2 \times 2$ unit-cell system, at 200 K, 250 K and 300 K, are also shown [15].

surface radiation. The radiation effect increases sharply with increasing temperature and the total heat loss is up to 20% of the input power Q_{in} at 300 K. The radiation from the sample Q_2 is small (no more than 1% of Q_{in}), due to the small surface area and the low temperatures. Among the radiation heat losses, Q_1 and Q_8 are the most significant, because the temperature of the heater is the highest and the copper wires have the largest surface area. Between 40 K and 100 K, the total heat loss is relatively small. The conduction through the wires is important below 40 K, due to the sharply increasing thermal conductivity of copper with decreasing temperature. The heat loss calculated by this model agrees well with the measured values at high temperatures. Note that the measured heat loss includes a different Q_2, which includes the radiation from the entire sample surface rather than the surface area between the heater and the cold cross-section. However, this difference is negligible (less than 1% of the input power), since the difference in these areas is small and the contribution of Q_2 is in general small.

3. Results and discussion

Fig. 4 shows the variation of the MOF-5 thermal conductivity with respect to temperature, from 6 K to 300 K. The experimental uncertainty of the absolute thermal conductivity is within ±15% (estimated by the standard error relation [13]). The uncertainty mainly results from the difficulty in the accurate determination of the effective cross-section area A (due to the small size and irregular shape of the sample) and the effective length of the heat flow path d (due to the junctions).

Since MOF-5 is a good dielectric, the thermal conductivity is from the contribution of phonons. The following processes are assumed to affect transport of phonons: grain-boundary scattering, lattice-defect scattering, and phonon–phonon scattering [14]. To analyze the data, the phonon mean free path λ_p is evaluated using the Debye model for specific heat capacity and the kinetic theory. The lattice thermal conductivity k is written as

$$k = \frac{1}{3} c_v u_{pg} \lambda_p = \frac{k_B}{2\pi^2 u_{p,g}^2} \lambda_p \left(\frac{k_B T}{\hbar}\right)^3 \int_0^{T_D/T} \frac{x^4 e^x}{e^x - 1} dx, \quad (4)$$

where k_B is the Boltzmann constant, $\hbar$ is the reduced Planck constant, T_D is the Debye temperature, $u_{p,g}$ is the phonon group velocity, and λ_p is the phonon mean free path. The mean free path λ_p is then given by

$$\lambda_p(T) = k \left[\frac{k_B}{2\pi^2 u_{p,g}^2} \left(\frac{k_B T}{\hbar}\right)^3 \int_0^{T_D/T} \frac{x^4 e^x}{e^x - 1} dx \right]^{-1}. \quad (5)$$

In the accompanying manuscript [15], we make an estimation of the Debye temperature ($T_D \simeq 102$ K) and the phonon group velocity ($u_{p,g} \simeq 1184$ m/s), which is independent of the thermal conductivity prediction. Using these values in Eq. (5), $\lambda_p(T)$ is plotted in Fig. 5.

From Fig. 4, below 70 K, the measured thermal conductivities of the different samples are not the same (we denote the sample with higher k as sample 1, and the other as sample 2), though both samples were transparent and sample 1 was only slightly clearer than sample 2 under the microscope. The mean free path of sample 2 is much smaller than that of sample 1 below 25 K, though they have similar dimensions. The mean free path of sample 2 reaches a limited value below 13 K, which is the typical effects of point defects (either inherent or due to thermal stresses resulting from cooling). However, λ_p of sample 1 continues to increase with decreasing temperature, suggesting this divergence is due to the different qualities of the samples. The peak in the thermal conductivity occurs at about 20 K (this

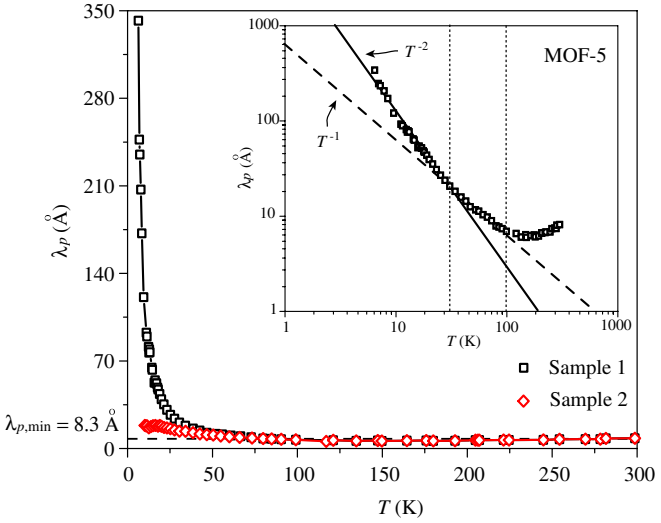

Fig. 5. Temperature dependence of the average phonon mean free path of MOF-5. The solid and dashed lines represent the dependence T^{-2} and T^{-1}, respectively. The results are for two different samples having different impurities and sizes.

is affected by the crystal quality). Below 20 K, the thermal conductivity increases sharply with increasing temperature, which is due to the excitation of more phonons at higher temperatures and is related to the increase of the specific heat [14]. From Fig. 5, the temperature dependence of λ_p changes at about 35 K, we find that $\lambda_p \propto T^{-2.16}$ (by fitting the mean free path between 6 K and 35 K). The typical interphonon scattering (U-process) will result in $\lambda_p \propto T^{-1}$ [14], and the dependence of T^{-2} suggests the effects of the lattice distortion [14,16]. The peak is just the result of the combination of the decreasing mean free path and the increasing specific heat, with the increase in temperature. From 35 K to 100 K, both k and λ_p decrease with increasing temperature, and λ_p shows a dependence $\lambda_p \propto T^{-1.17}$, suggesting the interphonon scattering dominates.

From 100 K to 300 K, the thermal conductivity only varies about 30%, considering the experimental uncertainties, the thermal conductivity exhibits a weak temperature dependence (similar to the behavior of amorphous phase). The MD predictions at 200 K, 250 K and 300 K, shown in Fig. 4, agree quite well with the measured value.

At 300 K, the thermal conductivity of MOF-5 is only 0.32 W/m K, a rather low value for crystals. This value can be compared with the thermal conductivities of other nanoporous crystals, such as the MD predicted value for the zeolites sodalite (3.53 W/m K), faujasite (2.07 W/m K), and zeolite-A (1.68 W/m K) [6]. The weak temperature dependence of the thermal conductivity is a common character for the nanoporous crystals [6]. Fig. 5 shows that λ_p is almost a constant above 100 K, indicating the minimization of phonon mean free path. Similar phenomena are found for other crystals [16]. The minimum mean free path of MOF-5 is about 8.3 Å, much smaller than the lattice constant (25.85 Å), but close to the cage size (7.16 Å). In the accompanying manuscript, we show that it is the carboxylate–carbon atom that limits the transport of the acoustic phonons, that is, the acoustic phonons are reflected at the connector between the cage and the bridge [15]. Considering most acoustic vibration modes lie in the cage, it is reasonable for the minimum λ_p to be close to the size of the cage. The low thermal conductivity and its temperature independence occur when most phonons reach their minimum mean free paths. In such a situation, the interphonon scattering cannot further reduce the phonon mean free paths and the energy is transmitted by activation or hopping of the localized modes, which is similar to the behavior of the amorphous phase [17].

4. Conclusions

The thermal conductivity of MOF-5 is measured for the first time over a wide temperature range, from 6 K to 300 K. The peak appears at about 20 K, and above 100 K the thermal conductivity is nearly temperature independent. The analysis of the mean free path suggests three regimes, namely, below 35 K, the lattice-defect scattering is an important scattering mechanisms. From 35 K to 100 K, the interphonon scattering dominates. Above 100 K, the phonon mean free path reaches its minimum, which is also found in the accompanying MD simulation as the suppression of the long-range acoustic phonons by the bridge structure [15].

Acknowledgements

This work has been supported by the US Department of Energy, Office of Basic Energy Sciences under grant DE-FG02-00ER45851.

References

[1] N.L. Rosi, J. Eckert, M. Eddaoudi, D.T. Vodak, J. Kim, M. O'Keeffe, O.M. Yaghi, Hydrogen storage in microporous metal-organic frameworks, Science 300 (2003) 1127.
[2] H. Li, M. Eddaoudi, M. O'Keeffe, O.M. Yaghi, Design and synthesis of an exceptionally stable and highly porous metal-organic framework, Nature 402 (1999) 276.
[3] J.L.C. Rowsell, A.R. Millward, K.S. Park, O.M. Yaghi, Hydrogen sorption in functionalized metal-organic frameworks, J. Am. Chem. Soc. 126 (2004) 5666.
[4] A. Griesinger, K. Spindler, E. Hahne, Measurements and theoretical modelling of the effective thermal conductivity of zeolites, Int. J. Heat Mass Transfer 42 (1999) 4363–4374.
[5] V.V. Murashov, M.A. White, Thermal properties of zeolites: effective thermal conductivity of dehydrated powdered zeolite 4a, Mater. Chem. Phys. 75 (2002) 178–180.
[6] A.J.H. McGaughey, M. Kaviany, Thermal conductivity decomposition and analysis using molecular dynamics simulations – Part II. Complex silica structures, Int. J. Heat Mass Transfer 47 (2004) 1799.
[7] R.W.G. Wyckoff, Crystal Structures, Interscience, New York, 1963.
[8] M. Eddaoudi, J. Kim, N. Rosi, D. Vodak, J. Wachter, M. O'Keeffe, O.M. Yaghi, Systematic design of pore size and functionality in isoreticular MOFS and their application in methane storage, Science 295 (2002) 469.

[9] M. Kaviany, Principles of Heat Transfer, John Wiley & Sons, Inc., New York, 2002.
[10] G.K. White, Experimental Techniques in Low Temperature Physics, Clarendon Press, Oxford, 1968.
[11] J.S. Dyck, W. Chen, C. Uher, L.D. Chen, X.F. Tang, T. Hirai, Heat transport in sb2-xvxte3 single crystals, J. Appl. Phys. 91 (2002) 3698.
[12] D.R. Linde (Ed.), CRC Handbook of Chemistry and Physics, CRC Press, 406 Boca Raton, 1992.
[13] L.W. da Silva, M. Kaviany, C. Uher, Thermoelectric performance of films in the bismuth–tellurium and antimony–tellurium systems, J. Appl. Phys. 97 (2005) 114903.
[14] R. Berman, Thermal Conduction in Solids, Clarendon Press, Oxford, 1976.
[15] B.L. Huang, A.J.H. McGaughey, M. Kaviany, Thermal conductivity of a metal-organic framework (MOF-5). Part I: Molecular dynamics simulations, Int. J. Heat Mass Transfer, this issue, doi:10.1016/j.ijheatmasstransfer.2006.10.002.
[16] K. Torizuka, H. Tajima, T. Yamamoto, Thermal conductivity of $(DMe-DCNQI)_2Li_{1-x}Cu_x$ $(0 \leqslant x \leqslant 0.14)$: Phonon propagation and the spin–peierls lattice distortion, Phys. Rev. B 71 (2005) 193101.
[17] G.P. Srivastava, The Physics of Phonons, Adam Hilger, New York, 1990.